bioRxiv preprint doi: https://doi.org/10.1101/2022.10.28.513987; this version posted October 30, 2022. The copyright holder for this preprint (which was not certified by peer review) is the author/funder. All rights reserved. No reuse allowed without permission.

# Functional Integration of 3D-Printed Cerebral Cortical Tissue into a Brain Lesion

Yongcheng Jin[1], Ellina Mikhailova[1], Ming Lei[2], Sally Cowley[3], Tianyi Sun[2], Xingyun Yang[1], Yujia Zhang[1], Kaili Liu[4], Daniel Catarino[4], Luana Campos Soares[4], Sara Bandiera[4], Francis G. Szele[4]*, Zoltan Molnar[4]*, Linna Zhou[1,5]* and Hagan Bayley[1]*

[1]Department of Chemistry, University of Oxford, Oxford, OX1 3TA, United Kingdom.

[2]Department of Pharmacology, University of Oxford, Oxford, OX1 3QT, United Kingdom.

[3]James and Lillian Martin Centre for Stem Cell Research, Sir William Dunn School of Pathology, University of Oxford, South Parks Road, Oxford, OX1 3RE, United Kingdom.

[4]Department of Physiology, Anatomy and Genetics, University of Oxford, Oxford, OX1 3PT, United Kingdom.

[5]Ludwig Institute for Cancer Research, Nuffield Department of Medicine, University of Oxford, Oxford, OX3 7DQ, United Kingdom.

*E-mail: francis.szele@dpag.ox.ac.uk, zoltan.molnar@dpag.ox.ac.uk, linna.zhou@chem.ox.ac.uk and hagan.bayley@chem.ox.ac.uk

Engineering human tissue with diverse cell types and desired cellular architectures and functions is a considerable challenge. The cerebral cortex, which has a layered cellular architecture composed of layer-specific neurons organised into vertical columns, delivers higher cognition through intricately wired neural circuits. However, current tissue engineering approaches cannot produce such structures. Here, we use a droplet printing technique to fabricate tissues comprising simplified cerebral cortical columns. Human induced pluripotent stem cells (hiPSCs) were differentiated into upper- and deep-layer neural progenitors, which were then printed to form cerebral cortical tissues with a two-layer organization. The tissues showed layer-specific biomarker expression and developed an integrated network of processes. Implantation of the printed cortical tissues into mouse brain explants resulted in substantial implant-host integration across the tissue boundaries as demonstrated by the projection of processes, the migration of

bioRxiv preprint doi: https://doi.org/10.1101/2022.10.28.513987; this version posted October 30, 2022. The copyright holder for this preprint (which was not certified by peer review) is the author/funder. All rights reserved. No reuse allowed without permission.

neurons and the appearance of correlated $Ca^{2+}$ signals. The approach we have developed might be used for the evaluation of drugs and nutrients that promote tissue integration. Importantly, our approach might be applied in personalised implantation treatments that restore the cellular structure and function of a damaged brain by using 3D tissues derived from a patient's own iPSCs.

## Main

Tissue regenerative therapies have gained tremendous recent interest and promise to provide alternative treatments for a wide range of difficult-to-treat injuries and diseases. The emergence of human induced pluripotent stem cells (hiPSCs) has the potential to generate the cell types that comprise all human tissues[1]. Importantly, autologous transplantation of iPSC-derived cells can minimise the immune response[2]. Here, we focus on the generation of neural tissues for implantation, although our technology is widely applicable.

Brain injuries, such as traumatic brain injury (TBI), can damage the cerebral cortex and cause catastrophic burden to patients and society. In 2018, it is reported that 69 million people globally suffer from TBI and 4.8 millions of these cases are severe [3,4], which leads to disabilities and an estimated mortality of 30% [5,6]. However, effective therapeutics are still absent for the treatment of brain injuries [7]. The implantation of neural progenitor cells and brain organoids into mice has been attempted for the repair of brain injuries [8,9]. However, the structure of the damaged brain tissue was not fully restored in these studies because the implanted dissociated cells or organoids did not provide the cellular architecture resembling natural brain anatomy. The cerebral cortex typically has a six-layer architecture composed of layer-specific neurons. Layers I-IV are designated upper layer, while Layers V-VI are the deep layers. Intracortical wiring of neural circuits between different layers [10,11], is believed to play an important role in higher cognition in mammals [12,13]. Rather than the implantation of dissociated hiPSCs-derived cells or organoids (lacking structural control), we suppose that the implantation of tissues resembling the cellular architecture of the damaged tissue will offer a more effective treatment. Here, we report a droplet printing technique that produces two-layered simplified model of cerebral

bioRxiv preprint doi: https://doi.org/10.1101/2022.10.28.513987; this version posted October 30, 2022. The copyright holder for this preprint (which was not certified by peer review) is the author/funder. All rights reserved. No reuse allowed without permission.

cortical columns. These constructs were implanted into lesions in live mouse brain explants. The implants undergo structural and functional integration, demonstrating a significant advance in tissue engineering *en route* to organ repair.

In brief, we first differentiated hiPSCs into two subtypes of neural progenitors (NPs), upper- and deep-layer neural progenitors (UNPs and DNPs; Fig. 1a, left column). These layer-specific NPs were then printed into layered cerebral cortical tissues using our 3D droplet printing technique, which enables the production of structurally defined and scaffold-free soft tissues composed of cells and extracellular matrix (ECM; Fig. 1a, middle column) [14-16]. The printed progenitor cells underwent maturation, including terminal differentiation, process outgrowth and migration. The layered structure was maintained *in vitro* and naturalistic layer-specific markers were expressed. The printed tissues were then implanted into lesions within mouse brain explants (Fig. 1a) and the cellular structure and integration were monitored over a week.

**Layered Structures by 3D-Droplet Printing**

The 3D droplet printer contains a piezo driver which generates mechanical pulses and ejects droplets from a printing nozzle (Extended Data Fig. 1a) [16]. The ejected droplets, containing ECM only (Fig. 1b) or ECM and cells (Fig. 1c,d), spontaneously acquire a lipid monolayer at the droplet/ oil interface, and contacting droplets formed droplet-interface bilayers (DIB; Fig. 1a, middle, and Fig. 1b). With computer-aided printing, the cell-containing droplets (diameter ~100 μm) can be patterned to produce various designs of droplet networks. For example, a 8x8x8 droplet network with RFP-labelled cells (Fig. 1e,f and Extended Data Fig. 1c,d) and a 12x12x12 droplet network with GFP-labelled cells enveloped by RFP-labelled cells (Fig. 1g) were printed. To produce material for implantation, we printed layer-specific neurons, RFP-labelled UNPs and non-labelled DNPs (see below), into a 16x8x8 two-layer droplet network (Fig. 1a bottom, h-j) with a height of ~1000 μm and width of ~500 μm, to from a simplified version of a cerebral cortex column comprising upper-layer and deep-layer segments [17]. Raising the temperature, from room to physiological, facilitated gelation and annealing of printed two-layer networks, containing either cells (Extended Data Fig.1d) or microbeads (Extended Data

bioRxiv preprint doi: https://doi.org/10.1101/2022.10.28.513987; this version posted October 30, 2022. The copyright holder for this preprint (which was not certified by peer review) is the author/funder. All rights reserved. No reuse allowed without permission.

Fig.1e).

To demonstrate that our printing technique might produce structures representing all six layers of the cerebral cortex [17], we applied a layer-by-layer sequential printing strategy (Extended Data Fig. 1f). Each layer, composed of an 8x8x8 droplet network, was labelled with a different colour (Fig. 1k and Extended Data Fig. 1g). In addition to printing sub-millimetre scale cubic structures, centimetre-scale structures with diverse shapes were also printed (Fig. 1l-n and Extended Data Fig. 1h).

**Generation of Layer-specific Neural Cells**

The differentiation of layer-specific cerebral cortical progenitor cells from hiPSCs was the essential first step towards fabrication of the two-layer cortical tissue. In humans and most other mammals, the layers of the cortex are formed in an inside-first-outside-last order. Deep-layer neurons, as the early product of cortical neurogenesis, divide asymmetrically from radial glia cells (RGCs) and migrate toward the cortical plate by radial migration from the ventricular zone [18]. Similarly, recent differentiation protocols have reported that, in early cultures, NPs primarily differentiate into deep-layer neurons (DNs), which can be phenotyped by the expression of the deep-layer marker CTIP2 [19,20].

To generate DNs, we applied a dual-SMAD inhibition differentiation method [21] to generate NPs in monolayer culture. Human iPSCs, reprogrammed from a healthy individual's somatic cells [21], were confirmed for their pluripotency. Immunostaining showed high expression of the pluripotency markers TRA-1-60, NANOG and OCT4 (Fig. 2b, left column and Extended Data Fig. 2a). We used a defined neural induction medium (NIM), containing the two SMAD inhibitors, LDN193189 and SB431542, to induce the hiPSCs into neural ectoderm lineage. The neural ectoderm cells were then cultured in neural maintenance medium (NMM), which enables the generation of NPs by 19 Days *in vitro* (DIV19). Further maturation was achieved by seeding NPs at a low density (100,000 cells/cm$^2$) and using neural terminal medium (NTM) containing the γ-secretase inhibitor (DAPT), which blocks the presenilin–γ-secretase complex [22] and prevents the downstream activation of Notch [23]. The inhibition of Notch pathway switches the

bioRxiv preprint doi: https://doi.org/10.1101/2022.10.28.513987; this version posted October 30, 2022. The copyright holder for this preprint (which was not certified by peer review) is the author/funder. All rights reserved. No reuse allowed without permission.

differentiation from glial to neuronal cell fates [24]. DAPT has been applied in various hiPSC differentiation protocols to facilitate neuron differentiation and maturation [25-27]. After 10 days of culture in NTM, DNs showed the features of mature neurons at DIV 29+ with a polarized morphology and the expression of the deep-layer marker CTIP2, but low expression of middle-upper (SATB2) and upper layer (CUX1 and BRN2) markers (Extended Data Fig. 3a,b).

Later in cortical neurogenesis, RGCs generate neurons that migrate radially into the cortical plate, passing through the DNs, to become upper-layer neurons (UNs) [18,28]. A recent protocol from Boissart, *et al.* addressed the generation of homogeneous UNs *in vitro* through prolonged pro-proliferative culture of NPs, which resembles the *in vivo* process of the late production of UNs from proliferating RGCs [27]. Following this protocol, we conducted an extended treatment of NPs with a growth factor cocktail, resembling the key steps of Boissart's protocol [27]. In contrast with the original protocol, we adopted small molecules for induction and the monolayer system in our neural differentiation protocol to reduce batch-to-batch variation. The growth factor cocktail included a combination of growth factors that support proliferation (FGF-2 and EGF) [29], and survival and maturation (BDNF) [27,30]. During the treatment, the cells retained progenitor morphology, and underwent 8-10 doublings from the beginning of neural induction until DIV 40. A representative culture on DIV 31 is shown in Fig. 2b (middle column). The UNPs at DIV 40 could then be harvested for further maturation culture or cryopreservation. For continual maturation of UNPs, the growth factors were withdrawn at DIV 40, and a further incubation in NTM containing DAPT over ten days was conducted to generate mature UNs at DIV 50+ (Fig. 2b, right column and Extended Data Fig. 4a-c). Without DAPT, however, the cells showed a non-polarised morphology which was similar to the UNPs, indicating failure to undergo maturation (Extended Data Fig. 4a). The UNs were morphologically similar to DNs (Extended Data Fig. 4a and Fig. 3a). However, immunofluorescent staining of DIV50+ UNs showed the expression of upper-layer markers CUX1, CUX2 and BRN2, and the middle-upper layer marker SATB2, whereas CTIP2 expression was rarely detected (Fig 2c and Extended Data Fig.4d). A quantitative analysis showed that DIV50+ UNs expressed CUX1, BRN2 and SATB2 at 68 ± 8%, 74 ±

bioRxiv preprint doi: https://doi.org/10.1101/2022.10.28.513987; this version posted October 30, 2022. The copyright holder for this preprint (which was not certified by peer review) is the author/funder. All rights reserved. No reuse allowed without permission.

7% and 70 ± 7%, respectively. In contrast, only 16 ± 4% cells expressed deep-layer marker CTIP2 (Fig. 2d).

To further confirm the identities of the DN and UN cells, we conducted gene expression analysis using a Real-time Quantitative Polymerase Chain Reaction (RT-qPCR). The treatment with the growth factor cocktail significantly upregulated CUX1 expression with a 20- and 22-fold change in DIV40+ UNPs and DIV50+ UNs compared to hiPSCs, whereas no upregulation detected in DIV19 DNPs. In addition, we did not detect CTIP2 expression changes in DIV40 UNPs. By comparison, DIV 47+ UNs in Boissart's original protocol also revealed ~20-fold upregulation of CUX1, along with an ~10-fold increase in CTIP2 expression [27]. PAX6, a neural stem cell marker [31], was identified in DIV19 DNPs indicating successful cortical neural induction. The expression of PAX6 was decreased in DIV40 UNPs and dropped further after maturation in DIV50+ UNs, with ~160-, 12- and 3-fold expression compared with hiPSCs in DIV19 DNPs, DIV40 UNPs and DIV50+ UNs, respectively. NESTIN, a neural marker, was upregulated over the differentiation and maturation process from a low level in DIV19 DNPs, and showed a 2-fold increase in DIV40 UNPs and a 7-fold increase in DIV50+ UNs compared with hiPSCs (Fig. 2e) [32].

By adapting the reported protocols [20,27], we produced two distinct progenitors, DNPs and UNPs, which gave rise to the corresponding mature layer-specific neurons: DNs and UNs. Our DIV 29+ DNs expressed the deep-layer marker CTIP2 but rarely expressed upper-layer markers. This result is consistent with reported protocols. For example, Shi's protocol producing ~40% CTIP2- and 5% BRN2-expressing neurons at DIV30 [20]. By comparison, Boissart's protocol generated over 70% of UNs expressing upper-layer markers CUX1 and BNR2 on DIV 47+ [27], consistent with the DIV 50+ UNs in this study (68% expressed CUX1 and 74% expressed BRN2).

**Printing Two-Layer Cerebral Cortical Tissue**

To fabricate functional cortical tissues, the progenitor cells, DNPs and UNPs, were harvested for printing. Progenitors, instead of mature neurons, were used because the progenitors were less sensitive to the dissociation procedure from 2D cultures compared

bioRxiv preprint doi: https://doi.org/10.1101/2022.10.28.513987; this version posted October 30, 2022. The copyright holder for this preprint (which was not certified by peer review) is the author/funder. All rights reserved. No reuse allowed without permission.

to mature neurons and were compact for printing. We printed the tissues in oil, followed by phase transfer into growth medium. For the first week of post-printing culture (WPP), the cortical tissues were incubated in NMM supplemented with a growth factor cocktail (FGF-2, EGF and BDNF) to facilitate tissue survival. At the end of 1 WPP, the growth-factor supplemented NMM was replaced with NTM to encourage the maturation of the cortical tissues. The tissues were harvested at 2, 4 and 8 WPP and assessed for morphology, cell migration, process outgrowth and gene expression (Fig. 3a).

We first fabricated deep-layer cortical tissues (8x8x8 droplet networks) from DNPs (Fig. 3b, top). The printed tissues were incubated in NMM supplemented with growth factors (Fig. 3b, middle and Extended Data Fig. 5a, left). A representative cortical tissue at 8 WPP was sectioned and immunostained to reveal the tissue structure and the cellular composition, which was visualized with neural markers: stem cell marker SOX2, general marker of young neurons TUJ1, deep-layer markers (CTIP2 and TBR1), and upper-layer marker (CUX1; Fig. 3b bottom, c and Extended Data Fig. 5b). CTIP2/TBR1-expressing DNs and sparse CUX1-expressing UNs were observed, which are comparable with *in vitro* differentiated human cortical neurons [20] and brain organoids[33].

To generate cortical tissues with two layers, we printed two 8x8x8 droplet networks side-by-side, one containing DNPs and the other UNPs, to give a 16x8x8 droplet network (Fig. 3d, top). We expected that the DNPs and UNPs would further differentiate during post printing culture to give the corresponding mature neurons, DNs and UNs, in the layers where they were printed. To determine 1) whether the two layers were preserved during post printing culture; and 2) whether the DNPs and UNPs were converted to DNs and UNs, we characterised the printed tissues at different differentiation time points.

Neuronal process outgrowth and migration are two important developmental phenomena of cortical neurogenesis. After two-weeks of culture, the printed cortical tissues remained in the desired two-layered architecture, as illustrated by bright-field images (Extended Data Fig. 5a, right) and immunofluorescence images with combined nucleus staining (DAPI, all cells) and RFP-labelled UNPs (Fig. 3d, middle). Further immunostaining of

bioRxiv preprint doi: https://doi.org/10.1101/2022.10.28.513987; this version posted October 30, 2022. The copyright holder for this preprint (which was not certified by peer review) is the author/funder. All rights reserved. No reuse allowed without permission.

sectioned 2 WPP cortical tissues revealed that the majority of cells in both layers expressed the neuronal marker TUJ1 and the neural stem cell marker SOX2 (Fig. 3d, bottom), indicating that the cells in both layers were neural. Z-projection images of the two-layered tissues at 8 WPP revealed that most of the neurons had acquired a polarized morphology with long processes, suggesting that neural differentiation and maturation has occurred in the printed tissue (Fig. 3e). A magnified view showed that the upper-layer neurons had produced processes projecting toward the deep layer (Fig. 3e). Neuron migration between layers was also found in the printed tissues, indicated by arrows in Figure 3e and Extended Data Fig. 5c. A movie of the 3D-reconstructed cortical tissue further illustrated the abundance of processes that crossed between layers (Supplementary Video 1). Comparison of the two-layer tissues at 2, 4 and 8 WPP revealed the dynamics of cross-layer process outgrowth and neuron migration (Fig. 3f). Quantitative analysis showed significant migration of RFP-labelled UNs into the deep-layer over 8 weeks of incubation, but no significant change of RFP-signal was found in the upper layer (Fig. 3g and Extended Data Fig. 5d).

Next, we assessed the spatial-temporal expression of general and layer-specific neural biomarkers to reveal the dynamics of neural maturation during post printing culture. Immunostaining of sectioned tissues at the three time points (2, 4 & 8 WPP) revealed a significantly higher population of cells in the upper layer compared to the deep layer that expressed the upper-layer marker CUX1 (78 ± 2 % v 37 ± 3 %, mean value over 2, 4 & 8 WPP) and the middle-upper layer marker SATB2 (68 ± 4 % v 39 ± 4 %). Conversely, a higher percentage of cells in the deep layer compared to upper layer expressed the deep-layer marker CTIP2 (35 ± 4 % v 10 ± 2%) at 2 WPP. The percentages of cells expressing CTIP2 in the deep and upper layer dropped to 18 ± 5% and 5 ± 0.2% respectively at 4 WPP and further fell at 8 WPP (4 ± 2 % and 3 ± 0.6%, respectively). This result is consistent with the previously reported observation in cerebral organoids where the population of cells expressing CTIP2 decreased from 30 to 105 days in culture after an initial increase during the first month, mimicking the temporal patterning observed in the mouse [34]. In addition, we found that a substantial population of cells (>90%) expressed neuronal marker TUJ1 at all time points in both layers, indicating that the majority of cells

bioRxiv preprint doi: https://doi.org/10.1101/2022.10.28.513987; this version posted October 30, 2022. The copyright holder for this preprint (which was not certified by peer review) is the author/funder. All rights reserved. No reuse allowed without permission.

in the printed tissues had committed to the neuronal lineage (Fig. 3h,i and Extended Data Fig. 5e,f). Together, these data demonstrate that the printed two-layer tissues retained the designed cellular architecture, with dynamic process outgrowth, cell migration. Further, the expected layer-specific marker expression was observed during the eight-week maturation process.

**Integration of Printed Cortical Tissue with Brain Explants**

Cultured organotypic brain explants preserve brain architecture and cellular function in an *ex vivo* environment [35,36]. We implanted printed cortical tissues into lesions in the cortex of mouse brain explants to assess their ability for tissue repair. We first printed the cortical tissues (on day -1) and cultured them for 1 day before implantation (Fig. 4a). On day 0, we prepared the brain explants and created an ~800-μm diameter circular lesion in the cerebral cortex. The explants were then cultured on Transwell inserts and the printed tissues were implanted into the lesion (Fig. 4a and Extended Data Fig. 5a,b). The implanted explants were then cultured under either condition A or B for one day, followed by DAPT treatment for 4 days (see Supplementary Table 1). Condition A is a nutrient-enriched formula modified from DMEM/F12 and Neurobasal medium containing a high glucose level of ~25mM [37], whereas condition B primarily consists of a commercially available BrainPhys medium with a physiologically relevant glucose level of ~2.5 mM. The high glucose concentration can inhibit neuron differentiation through oxidative and endoplasmic reticulum stress [38]. Previous reports have indicated the superior performance of BrainPhys medium compared to DMEM/F12 and Neurobasal medium on the 2D culture of hiPSC-derived neurons in supporting neuronal survival and function, such as frequent action potential firing and long-term electrical activity [37]. To evaluate the effects of condition A, condition B and DAPT on the integration of the implant, process outgrowth and neuron migration from the implants into the host were measured (Fig. 4b).

Fluorescent confocal imaging revealed process outgrowth and neuron migration from the implant towards the host, indicating that the printed tissues had integrated into the brain explant (Condition B, no DAPT; Fig. 4c). Live/dead staining showed that the cells in the brain explants were 86 ± 3 % viable at 5 days post-implantation (DPIs; Extended Data

bioRxiv preprint doi: https://doi.org/10.1101/2022.10.28.513987; this version posted October 30, 2022. The copyright holder for this preprint (which was not certified by peer review) is the author/funder. All rights reserved. No reuse allowed without permission.

Fig. 6c,d). The viability of the implants was similar as indicated by their RFP expression (Fig. 4c). Analysis of the RDP-labelled neurons also revealed process outgrowth and neuron migration from 1 to 5 DPIs (Fig. 4d). Profile plots of fluorescent intensity revealed the extent of process outgrowth at 1DPI (220 μm) and 5 DPI (405 μm; Fig. 4e).

Process outgrowth and neuron migration is regulated by microenvironmental cues during neurogenesis [39,40]. We, therefore, hypothesised that process outgrowth and cell migration might respond to different nutrient conditions and small molecular treatment, such as DAPT. To address this, we cultured implanted explants under four conditions: condition A and B, with and without DAPT. Using fluorescent confocal imaging, we found differences in the distance of outgrowth and migration under the four conditions at 5DPIs (Fig. 4f). Quantitative analysis showed a significant increase in the distance of process outgrowth in condition B (434 ± 41 μm) compared to condition A (265 ± 30 μm). Interestingly, DAPT treatment led to further increases in the distance for both condition A (increased by 153 μm to 418 ± 70 μm) and condition B (increased by 287 μm to 721 ± 71 μm; Fig. 4g and Extended Data Fig. 6e). Therefore, our data illustrated that the implanted explants can be used to evaluate the effect of nutrients and small molecule treatment on implantation.

We also examined the influence of the duration of the pre-implantation incubation of the printed tissues. We compared the distance of process outgrowth and neuron migration from the implants with 1- or 14-days pre-implantation incubation in condition B. The outcome suggested that a 14-day pre-implantation culture of cortical tissues can extend implant-to-host process outgrowth (Fig. 4h). We found an increase in process outgrowth of 222 μm to 656 ± 63 μm at 5 DPIs, compared with the implants that had undergone a 1-day pre-implantation incubation (Fig. 4i and Extended Data Fig. 6e).

Under high magnification, we identified individual neurons migrating across the implant-host boundary (Fig. 4j). Quantitative analysis was conducted by counting the number of RFP-labelled neurons in an area between 200 and 400 μm away from the implant. The analysis showed 20 ± 2, 17 ± 3 and 18 ± 3 RFP-labelled neurons/0.1mm$^2$ migrated into the host brain explant at 5 DPIs from implants composed of UNs, DNs, and 14 days pre-

bioRxiv preprint doi: https://doi.org/10.1101/2022.10.28.513987; this version posted October 30, 2022. The copyright holder for this preprint (which was not certified by peer review) is the author/funder. All rights reserved. No reuse allowed without permission.

cultured DNs respectively. The migration of UNs was observed over three time points: 1, 3 and 5 DPIs (1.4 ± 0.4, 12 ± 4, 20 ± 2 neurons/0.1mm$^2$ respectively).

**Functional Integration of Printed Two-layer Cortical Tissue with Brain Explants**

Effective therapies using stem cell-derived cortical tissue for brain repair has not been established. A critical challenge is the difficulty in forming functional connections between implants and the host brain. Here, we printed cortical tissues with a size compatible with explants of the cerebral cortex of P8 mice (800-1000 μm) [41] and a simplified laminar architecture consisting of deep and upper layers. The two-layered cortical tissue was then implanted into the lesioned cortex of a mouse brain explant. Importantly, the orientation of the implanted tissues was matched with the cortex of the host; the deep layer of the implant was implanted into the ventral region of the cortex and the upper layer into the dorsal region. Integration between the implants and host was evaluated through the extent of process outgrowth and neuron migration from the implant towards the host (Fig. 5a,c and Extended Data Fig. 6f). Quantitative analysis of process outgrowth and neuron migration at 1, 3 and 5 DPIs showed an increase in process projection distance over the culture periods: 85 ± 14 μm, 336 ± 22 μm to 419 ± 22 μm, respectively (Fig. 5b). Further, immunostaining showed human-specific neural marker HNCAM expression in both layers confirming the human origin of the implanted neurons, while RFP expression was sharply lower in the upper layer compared to the deep layer, indicating that the two-layer pattern had been maintained in the implant (Fig. 5 d,e).

In the nervous system, correlated $Ca^{2+}$ oscillations of cells in connected neuronal circuits are necessary for brain functions [42-44]. To evaluate the functionality of the implanted cortical tissues, we performed $Ca^{2+}$ imaging with Fluo-4, a fluorescent calcium indicator. Time-lapse recordings of implanted explants revealed spontaneous $Ca^{2+}$ oscillations of cells in both the implant and the host at 5 DPIs (Fig. 5f). Simultaneous calcium ion fluctuations in adjacent cells, suggested potential correlation between these cells (Fig. 5g). To seek correlations of calcium oscillations between implant and host, we recorded $Ca^{2+}$ signals at the implant/ explant interface (Fig. 5h and Supplementary Video 2). By applying the correlation calculation method reported by Ko *et al*. [45], we found that the

bioRxiv preprint doi: https://doi.org/10.1101/2022.10.28.513987; this version posted October 30, 2022. The copyright holder for this preprint (which was not certified by peer review) is the author/funder. All rights reserved. No reuse allowed without permission.

neurons exhibited $Ca^{2+}$ oscillations with a correlation factor of R>0.1 at 5 DPIs, suggesting a functional connection between the implant and the host (Fig. 5i and Extended Data Fig. 7a). Additional similarity matrices and correlated network analyses supported the existence of multiple neuronal communities with correlated firing patterns (Fig. 5j and Extended Data Fig. 7b,e). Further $Ca^{2+}$ imaging (Fig. 5k and Extended Data Fig. 7c,d) and correlated network assessment (Fig. 5m and Extended Data Fig. 7e) on 5 DPI implanted explants showed correlated cell pairs within the implant and the host, and across the implant/ explant boundary. Specifically, we demonstrated a group of regions of interest (ROIs) with correlated $Ca^{2+}$ traces between implant and host (Fig. 5n). Overall, for 3-5 DPI implanted explants, we found 4.4 ± 0.7% correlated host-to-host cell pairs, 1.6 ± 0.3% host-to-implant cell pairs and 2.0 ± 0.9% implant-to-implant cell pairs (Fig. 5o). These data show that potential functional connections exist between the printed two-layered cerebral cortical tissue and the host tissue.

## Discussion

Here, we demonstrate that droplet-based 3D-printing can be used to produce tissues with the architecture of a simplified two-layer cerebral cortical column. The identity and structure of the deep and upper layers were maintained during *in vitro* culture after printing. During this period, process outgrowth, neuron migration and maturation were observed. Subsequent implantation of the printed cortical tissues into brain explants demonstrated the formation of structural and functional connections between the implant and the host.

The emergence of hiPSCs and recent advances in stem cell differentiation, particularly those producing deep- and upper-layer specific neurons [20,27] encouraged us to fabricate, for the first time, a layered cortical tissue in three dimensions. Although we demonstrated that our droplet-printing technique is capable of producing six-layered structures, mimicking the complex human cerebral cortex architecture, current hiPSCs techniques have not produced populations of neurons representing all six layers. Further advances in the generation of layer-specific cortical neurons, along with our droplet printing technique, will enable the fabrication of more fine-grained and realistic 3D *ex vivo* cortical tissues for better understanding the mystery of how intracortical human neuron circuits

bioRxiv preprint doi: https://doi.org/10.1101/2022.10.28.513987; this version posted October 30, 2022. The copyright holder for this preprint (which was not certified by peer review) is the author/funder. All rights reserved. No reuse allowed without permission.

develop and lead to higher cognition [10,11].

In the current study, we printed neural progenitors, DNPs and UNPs, instead of their mature descendants. These progenitors differentiated in the printed tissues during post printing culture. This strategy allowed us to avoid the difficulties associated with handling mature neurons which are known to be sensitive to dissociation from culture vessels and would likely be damaged in the 3D printing process due to their sensitivity to physical stress, changes in temperature, and changes in osmolarity [46].

Interestingly, after printing, the DNPs and UNPs continued to mature in the host towards DNs and UNs respectively, despite the fact that they were in a common growth medium. The use of lineage-committed progenitors represents a novel strategy for the fabrication of 3D tissues. Recently, the Lewis group reported a co-differentiating strategy in 3D tissues derived from two types of hiPSCs, transfected with either neural or endothelial-associated transcription factors (TFs), to produce vascularised neural tissues[47]. Although the study produced patterned neural tissues containing distinct cell types, it relied on lentivirus-based genetic modifications, which might have limited application potential in implantation therapies [48,49]. In our strategy, the production of neural tissues containing distinct types of neurons without genetic manipulation, reduces concerns over clinical safety, and might be applied to the construction of other tissues containing multiple cell types.

The transplantation of dissociated human neurons into the mouse brain has been reported in several studies, which have demonstrated the survival of injected cells, pathway generation and implant-host connections [8,50]. However, the transplantation of dissociated cells has not been reported to restore the architecture of lost tissue, for example, the laminar structure of the lesioned cortex. With droplet printing, an implant can be designed to emulate the dimensions, orientation, cellular composition and structure of the lost tissue. Particularly in the case of a large lesion, the implantation of replacement tissue with matched 3D shape and cellular architecture will provide a precise treatment. In the present study, printed two-layer cortical tissues were implanted into live

bioRxiv preprint doi: https://doi.org/10.1101/2022.10.28.513987; this version posted October 30, 2022. The copyright holder for this preprint (which was not certified by peer review) is the author/funder. All rights reserved. No reuse allowed without permission.

mouse brain explants, leading to structural integration, based on implant-to-host process outgrowth and neuron migration, and functional integration shown by calcium oscillations correlated between the implant and the host. Considering the short period of post-implantation culture, we presume that the functional connections are a result of the early establishment of volume transmission, a neuronal signal transmission mechanism conducted by non-synaptic release of neurotransmitters, which diffuse through the extracellular space [51,52]. Implantation after longer post-implantation incubation times might lead to more advanced functional repair, an aim of our future work. Further research could take advantage of potential advances in neural differentiation that produce further layer-specific neurons and thereby more realistic cortical tissues. Progenitors derived from patients' own cells might also be used to produce implants to treat currently incurable brain damage.

## Methods

All catalogue numbers of materials are incorporated in Supplementary table1, 2 and 3.

### hiPSC differentiation

*Cell lines.* The iPSC lines used in this study were kindly provided by Dr Sally Cowley (James Martin Stem Cell Facility, Oxford). We used three AH016-3 lines: unlabelled, RFP-labelled, and GFP-labelled [21].

*Maintenance.* iPSC lines were maintained and expanded at 37°C in 5% $CO_2$ in mTeSR™Plus medium (Stemcell Technologies) on 1:100 diluted Geltrex (Thermo Fisher)-coated plates with daily medium changes and passaging every 3-4 days with releasing agent ReLeSR (Stemcell Technologies).

*DNP differentiation.* On DIV-1, hiPSCs were passaged 1:1 or 3:2 after release as small clusters with 0.5 mM EDTA. To achieve this, cells were washed with Dulbecco's phosphate-buffered saline (DPBS; Gibco) and treated with 0.5 mM ethylenediaminetetraacetic acid (0,5 EDTA; Life Technologies) for 7-10 min. After aspiration of the EDTA, cells were lifted with mTeSR™Plus medium. Floating cells were

bioRxiv preprint doi: https://doi.org/10.1101/2022.10.28.513987; this version posted October 30, 2022. The copyright holder for this preprint (which was not certified by peer review) is the author/funder. All rights reserved. No reuse allowed without permission.

collected and replated onto Geltrex-coated plates in mTeSR™Plus. On DIV0, 100% confluent hiPSCs were induced with Neural Induction Medium (NIM, Supplementary Table 1). The medium was exchanged with fresh NIM daily until DIV7. On DIV7, the cells were passaged 1:2 using 0.5 mM EDTA, replated, and cultured in NIM supplemented with 10 µM Y-27683 (Stemcell Technologies). On DIV8, the culture medium was changed to Neural Maintenance Medium (NMM, Supplementary Table 1). On DIV12, cells were passaged 1:2 again using EDTA as described above. On DIV 16, cells were passaged 1:2 using Accutase (Life Technologies). The cells were washed with DPBS first and then treated with 1 mL Accutase at 37°C for 5-7 mins. Then, an additional 3 mL DMEM/F12 medium were added (Life Technologies), followed by centrifugation for 5 min at 200 *g*. The cell pellet was resuspended with NMM supplemented with 10 µM Y-27683 and replated on Geltrex-coated plates. On DIV19, hiPSC-DNPs were passaged for either cryopreservation as cell stocks or replating for terminal maturation. For cryopreservation, DNPs were treated with 10 µM Y-27683 for three hours before dissociation with Accutase. Cell pellets were resuspended in 1 mL pre-chilled freezing medium containing 90% Fetal Bovine Serum (FBS, Gibco) and 10% DMSO (Sigma). The resuspended DNPs were transferred into cryopreservation vials and slow cooled in Freezing Containers (Thermo Scientific) at -80°C overnight, before transfer into liquid nitrogen for long-term preservation.

*UNP differentiation.* DIV19 DNPs were cultured in NMM supplemented with a growth factor (GFs) cocktail containing 10 ng/mL Fibroblast Growth Factor-2 (FGF-2), Epidermal Growth Factor (EGF) and Brain-derived Neurotrophic Factor (BDNF) (NMM+GFs, Supplementary Table 1). The culture medium was exchanged with fresh medium daily. Once the progenitors reached 100% confluency, they were passaged 1:2 using Accutase as described under *DNP differentiation*. The centrifuged cells were resuspended with NMM+GFs and replated. Passaging was performed approximately every 5 days until DIV 40. The DIV 40 UNPs were either cryopreserved or cultured for terminal maturation as described for DNPs.

*Maturation.* To thaw cryopreserved DNPs or UNPs, the frozen cells were placed in a 37°C

bioRxiv preprint doi: https://doi.org/10.1101/2022.10.28.513987; this version posted October 30, 2022. The copyright holder for this preprint (which was not certified by peer review) is the author/funder. All rights reserved. No reuse allowed without permission.

water bath. When the cells had nearly thawed, they were transferred to NMM and centrifuged at 200 *g* for 4 min. The cell pellet was re-suspended in NMM with 10 μM Y-27683 and plated into one well of a Geltrex-coated 6-well plate. The cells were cultured for 2 days with a medium change after one day.

Then, the cells were passaged by using Accutase and replated at a concentration of 100,000/cm$^2$ on 8- or 96-well plates with Neural Terminal Medium (NTM, Supplementary Table 1) supplemented with 10 μM Y-27683. The culture medium was exchanged with fresh supplemented NTM every 3-4 days. After 10 days, mature neurons had been generated and were ready for assessment.

**Immunocytochemistry**

*Immunostaining and quantification.* DNs and UNs were cultured on Geltrex-coated 96 Well Black Polystyrene Microplates (Corning), washed with DPBS and fixed with 4% paraformaldehyde (PFA) at room temperature for 15 min. After fixation, the cells were washed 3 times with ice-cold DPBS, permeabilized by 0.1% Triton X-100 in DPBS (DPBST) for 20 min and washed again 3 times with DPBS. Then, the cells were blocked from non-specific binding with 10% goat serum diluted in DPBST for 60 min at room temperature. Subsequently, the neurons were incubated with primary antibodies diluted in 1% goat serum in DPBST in a humidified chamber overnight at 4°C. Then, the neurons were washed with DPBST three times and incubated with secondary antibodies diluted in 1% goat serum in DPBST for 2 h at room temperature. Information on the antibodies used is in Supplementary Table 3. After incubation, the cells were washed three times with DPBST and once with DPBS at room temperature. Then the neurons were mounted with Antifade Mounting Medium with DAPI (Abcam). The neurons could be examined directly or stored in the dark at 4°C for later examination. For the quantification of cells expressing specific cortical neuronal markers, at least two images with a field of view that included over 40 cells were made. The cells were counted and the numbers were averaged for biologically independent sample. Associated consumables are listed in Supplementary Table 2.

bioRxiv preprint doi: https://doi.org/10.1101/2022.10.28.513987; this version posted October 30, 2022. The copyright holder for this preprint (which was not certified by peer review) is the author/funder. All rights reserved. No reuse allowed without permission.

## Real-time quantitative PCR (qPCR)

Neurons were snap-frozen by putting a pellet of cells in a 15 mL centrifuge tube into powdered dry ice and stored at -80°C, after thawing for qPCR assessment, total RNA was isolated using a Monarch@ Total RNA miniprep Kit (New England BioLabs) according to the manufacturer's instructions. An additional in-tube DNase I digestion was performed to avoid the amplification of genomic DNA. RNA concentrations and quality were assessed by using a Nanodrop spectrophotometer. The RNA was reverse transcribed by using the LunaScript RT SuperMix Kit (New England BioLab). Quantitative PCR assays were set up by loading primer mixes and cDNA into wells of a 96-well plate in triplicate, followed by the addition of Luna Universal qPCR Master Mix (New England BioLabs). qPCR reactions were performed using the ProFlex PCR System (Applied Biosystem). Conditions were selected according to the manufacturer's suggestions (LunaScript). Relative gene expression values were determined by averaging the results of two to three technical replicates and comparing the $C_t$ values for genes of interest with those of the control gene (18S RNA) using the $\Delta\Delta C_t$ method. Associated consumables and Primers are listed in Supplementary Tables 2 and 3.

## Droplet-printing and tissue culture

*Set up.* The printer was upgraded from that reported previously[14,15]. Two microscopes were used to provide both front and side views, allowing a precise localisation of droplets and the alignment of multiple networks. 3D printing was performed in a temperature- and humidity-controlled cold room. Matrigel-based bioink was printed at ~4°C and ~80% humidity. Glass printing nozzles were pretreated with (3-aminopropyl)trimethoxysilane (Sigma) to provide a hydrophilic coating, which prevented the leakage of bioink and stopped oil entering the nozzles. The printing oil bath contained 2 mg/mL DPhPC (1,2-diphytanoyl-sn-glycero-3-phosphocholine, Avanti) in a mixture of undecane and silicone oil AR20 1:4 (v/v) (both from Sigma). Associated consumables are listed in Supplementary Table 2.

*Bioink preparation and droplet printing*. Cells were suspended after dissociation with Accutase. Cell number and viability were assessed after trypan blue staining (Life

bioRxiv preprint doi: https://doi.org/10.1101/2022.10.28.513987; this version posted October 30, 2022. The copyright holder for this preprint (which was not certified by peer review) is the author/funder. All rights reserved. No reuse allowed without permission.

Technologies) by either manual counting with a hemocytometer or by using a Countess II automated cell counter (ThermoFisher). The cell suspension was then centrifugated at 200 *g* for 5 min, followed by removal of the supernatant. Pre-thawed Matrigel at 4°C was then added to the pellet and the cells were resuspended on ice to to generate the bioink, which was then loaded into printer nozzles at ~4°C. Printing was performed by using custom printing-control software. The printing process took 15 min to generate an 8X8X8 droplet network. Patterned networks were printed either with two nozzles or by reloading a single nozzle.

*Phase transfer.* A previous protocol [15] was optimised. The glass cuvette containing printed networks at 4°C was placed in a room-temperature water bath for 20 min before transfer to a tissue culture incubator at 37°C for 1 h. Two thirds of the oil was then aspirated and replaced with a mixture of undecane and silicone oil AR20 (1: 4 v/v). The exchange process was repeated five times to dilute the lipid. Culture medium was then added drop-by-drop and exchanged four times to remove residual oil. Phase-transferred tissue was pipetted into 12-well or 24-well plates for culture.

*Culture of printed tissues.* Printed neural cortical tissues were cultured in NMM supplemented with FGF-2, EGF and BDNF (all at 10 ng/mL) and 100 U/mL Penicillin-Streptomycin (ThermoFisher) for the initial 7 days. 10 μM Y-27683 was included for the first 3 days to prevent apoptosis. Then, the cortical tissue was incubated in NTM containing 100 U/mL Penicillin-Streptomycin for up to 8 weeks. Half of the medium was exchanged with fresh medium every 3 days.

**Immunohistochemistry of printed tissues**

*Tissue sections.* Printed tissues were fixed in 4% v/v paraformaldehyde for 1 h at room temperature and washed with DPBS three times. The fixed tissues were embedded in optimal cutting temperature compound (OCT, VWR) with dry ice and sectioned using a cryostat (Leica, CM1860 UV) to generate 30-μm-thick sections on glass slides for immunostaining.

bioRxiv preprint doi: https://doi.org/10.1101/2022.10.28.513987; this version posted October 30, 2022. The copyright holder for this preprint (which was not certified by peer review) is the author/funder. All rights reserved. No reuse allowed without permission.

*Immunostaining.* The tissue sections were circled with a PAP pen (Merck) to create a hydrophobic barrier so that reagents could be localized. The sections were then stained according to "Immunocytochemistry" (see above). After staining, tissue sections were mounted in Mounting Medium with DAPI (Fluoroshield, Abcam) and sealed with coverslip and nail polish for storage at 4°C storage. Fluorescence visualization was carried out with a confocal microscope and analysed with ImageJ. For quantification, three random fields were counted in each of the deep and upper layers and averaged for each biologically independent sample at 2-, 4- and 8-weeks post-printing culture. Three biologically independent samples were counted for each marker and timepoint.

**Implantation into mouse brain explants**

Cerebral cortical tissues were printed 1 day before mouse brain slices were obtained. The next day, P8 C57BL/6J mice were killed by cervical dislocation in accordance with the Animals Scientific Procedures Act (1986) under licence no. PP8557407. Brains were harvested and kept in ice-cold carbogen-saturated (95% $O_2$/ 5% $CO_2$) Earle's Balanced Salt Solution (EBSS, Life Technologies). Coronal slices (300 µm) were obtained by sectioning with a compresstome (Precisionary, VF-310-0Z). The brain slices (explants) were cultured on 0.4-µm Millicell-culture inserts (Merck Millipore) in six-well plates. On the same day, a biopsy punch (EMS) with 500-µm inner and 800-µm outer diameter was used to punch a lesion in the cortex of the explant. The 800-µm circle spanned most of the thickness of the P7 mouse (~800-1000 µm, Allen Brain Atlas) [41]. The printed cortical tissue was then implanted into the lesion in the natural orientation (upper layer out). The implanted explants were maintained in culture medium under either nutrient condition A or nutrient condition B (Supplementary Table 1) at 37°C under 5% $CO_2$. On Day 2, DAPT was added directly to the cultures without a medium change to a final concentration of 10 nM. The culture medium was then changed every 3 days. Associated consumables are listed in Supplementary Table 2.

**Characterization of implanted explants**

*Whole-mount immunostaining.* On day 1, 3 or 5 post-implantation, brain explants were fixed in 4% v/v paraformaldehyde for 1 h at room temperature. The immunostaining

bioRxiv preprint doi: https://doi.org/10.1101/2022.10.28.513987; this version posted October 30, 2022. The copyright holder for this preprint (which was not certified by peer review) is the author/funder. All rights reserved. No reuse allowed without permission.

protocol was similar to that in "Immunohistochemistry of printed tissues". In short, the explants were washed with DPBS, permeabilized by using 0.5% Triton X-100 in DPBS (DPBST-0.5%) for 20 min, blocked with 10% goat serum in DPBST-0.5% for 60 min and immunostained with primary antibodies in 1% goat serum in DPBST-0.5% overnight at 4°C. After three DPBST-0.5% washes, the explants were stained with secondary antibody (see Supplementary Table 3) in 1% goat serum in DPBST-0.5% for 2 h at room temperature, followed by DAPI staining (1 µg/mL) for 1 h and three DPBST-0.5% washes. The immunostained explants were stored in the dark in DPBS at 4°C before imaging.

*Live/dead assay.* Implanted explants at 5 DPIs were incubated with 2.5 µM Calcein-AM (Cambridge Biosciences Ltd) and 5.0 µM propidium iodide (Sigma Aldrich) for 30 min before imaging. Three randomly selected cortical regions of the explants were imaged. Images were processed in ImageJ and counted manually.

*Calcium imaging.* A Fluo-4 Direct calcium assay kit (Invitrogen) was used according to the manufacturer's instructions to determine calcium activities. In short, explants on culture inserts (0.4 µm Millicell, Merck Millipore) were incubated with a mixture of BrainPhys™ Imaging Optimized Medium (Stemcell Technologies) and Fluo-4 calcium imaging reagents (1:1 v/v) for 1 h at 37°C. After incubation, the brain explants were harvested by cutting the semi-permeable membrane from the culture insert and placed upside down on imaging dishes (Ibidi). Spontaneous calcium fluctuations were recorded at 37°C by fluorescence confocal microscopy (Leica SP5) at 1 frame per 1.29 s.

**Calcium Imaging Analysis**

All videos were recorded at 1.29s/frame. For the analysis of calcium imaging (Fig. 5g, i, m, n and o), pre-processing was performed in ImageJ. Neurons were identified as bright objects and manually selected as ROIs. The fluorescence changes of each ROI over the recording period were extracted (termed fluorescence traces) and exported as csv files for further analysis with Excel. Subsequently, functional neuron connection analysis was performed based on the method reported by Ko et al[45]. Briefly, for each fluorescence trace, fluorescence at a given time t ($F_t$) was normalized as $\Delta F/F_0$. $F_0$ is the averaged

bioRxiv preprint doi: https://doi.org/10.1101/2022.10.28.513987; this version posted October 30, 2022. The copyright holder for this preprint (which was not certified by peer review) is the author/funder. All rights reserved. No reuse allowed without permission.

fluorescence value for the initial 10 frames. $\Delta F = F_t - F_0$. the fluorescence trace was smoothed by averaging six-frames ($\Delta F_t/F_0 = (\Delta F_{t-2}+\Delta F_{t-1}+\Delta F_t+\Delta F_{t+1}+\Delta F_{t+2}+\Delta F_{t+3} /F_0) / 6$). Then, background fluorescence was filtered out from each fluorescence trace by applying a threshold which was defined as median value of the trace, with an addition of 0.02-0.05 to make it stricter. Next, each background filtered trace was normalized to '0-1' (with the maximum $\Delta F/F_0$ assigned as '1' and the minimum $\Delta F/F_0$ as '0'). Pearson's correlation between pairs of traces was calculated in Excel ('Data Analysis> Correlation') to generate a correlation matrix containing Pearson's correlations between all possible trace pairs. To visualise the correlations, the matrix was imported into R (Rstudio1.3.1093) by applying the plotting R package igraph (v1.3.2). We used circles to represent the location of ROIs and lines to represent the Pearson's correlation between pairs of ROIs. Following the Ho's report[45], neuron pairs with Pearson's correlation > 0.1 are defined as correlated. A blue-to-purple colour scheme was applied to the lines to represent low-to-high values of the Pearson's correlations.

To generate the similarity matrix in Fig. 5j, pre-processing, movement correction and ROI detection of calcium imaging videos were performed automatically in the default settings of an open-source toolbox in MATLAB, termed NETCAL (version 8.4.1). Subsequently, NETCAL extracted fluorescence traces for all ROIs. These traces were then smoothed and a similarity matrix of all traces was generated by using default settings in NETCAL. NETCAL automatically arranged the highly correlated ROIs to the top left of the graph, and the weakly correlated ROIs to the bottom right of the graph.

**Process outgrowth and neuron migration analysis**

*For printed two-layer tissues*. Sectioned two-layer tissues were analysed in ImageJ. The RFP coverage (Fig. 3f,g) was measured as the ratio of the RFP-labelled area over the total area of the deep layer, which was defined and quantified by drawing a box covering the deep-layer region and using the 'threshold' and 'measurement' tool in ImageJ. Individual migrating neurons were manually selected by using the 'cell counter' plugin in ImageJ. RFP-labelled neurons with apparent cell bodies and co-localised DAPI staining falling in the distance range of 200 to 400 μm away from the upper-layer boundary were

bioRxiv preprint doi: https://doi.org/10.1101/2022.10.28.513987; this version posted October 30, 2022. The copyright holder for this preprint (which was not certified by peer review) is the author/funder. All rights reserved. No reuse allowed without permission.

651 counted as migrated neurons (Fig. 3g).

652

653 *For implanted explants.* The distance of process outgrowth in the implanted explants was
654 measured as the farthest distance from the implant that RFP signals could be detected
655 from single-layer implants and HNCAM signals from two-layer implants. The upper layer
656 identity in two-layer tissues was confirmed from the extent of RFP expression. In imageJ,
657 the fluorescence intensities were plotted with 'profile plots' and the width of the grey value
658 decreasing phase was used to represent the outgrowth distance. Individual migrating
659 neurons were counted by the 'cell counter' plugin in imageJ. RFP-labelled neurons with
660 apparent cell bodies and co-localised DAPI staining falling in the distance range of 200
661 to 400 μm away from the implant-host boundary were counted as migrating neurons
662 (Figure 4j,k).

663

664 **Microscopy and image processing**

665 Differentiated neurons were imaged using fluorescence confocal microscopes (Leica
666 LSM780 and Leica SP5) and epi-fluorescent microscopes (Leica DMI 8 and Nikon Eclipse
667 Ni-E). Printed cortical tissues were imaged using a fluorescence confocal microscope
668 (Leica LSM780). Implanted explants were imaged using fluorescence confocal
669 microscopes (Leica LSM780 and LSM980). Images were analysed by using ImageJ
670 (version 2.1.0/1.54c).

671

672 **Statistics**

673 Data in text are presented as mean ± standard error of the mean (S.E.M.). Data in figures
674 are presented either as mean ± S.E.M. (Fig. 2d,e, Fig. 3g,i, Fig. 4 g,i, Fig. 5b and
675 Extended Data Fig. 6d) or mean ± Standard Deviation (SD) range (Fig. 5d). For Fig. 2d,e
676 and Fig. 3g,i, biological replicates n = 3. For Fig. 4k, biological replicates n ⩾3. For Fig.
677 4g, biological replicates n ⩾4. For Fig. 4i, biological replicates n ⩾5. For Fig. 5b,d,
678 biological replicates n ⩾3. For Fig. 5o, biological replicates n = 3. Statistical analysis was
679 performed using GraphPad Prism 9. A detailed statistical analysis is listed in
680 Supplementary Table 4.

681

bioRxiv preprint doi: https://doi.org/10.1101/2022.10.28.513987; this version posted October 30, 2022. The copyright holder for this preprint (which was not certified by peer review) is the author/funder. All rights reserved. No reuse allowed without permission.

## Data availability

All data generated or analysed during this study are included in the paper and its Supplementary Information. Source data are available on request.

## Acknowledgements

This research was supported by a European Research Council Advanced Grant (SYNTISU) and the Oxford Martin School Programme on 3D Printing for Brain Repair.

## Author Contributions

Y.J., F.G.S., Z.M., L.Z. and H.B. conceived, designed and guided the project. Y.J. performed most experiments and analysis. Y.J., E.M. and L.Z. performed iPSCs culture. S.C. provided hiPSCs lines and advice on differentiation. Y.Z. and X.Y. assisted with confocal imaging and droplet printing. X.Y. assisted with tissue staining and Y.Z with coding and statistics. M.L. and T.S. performed animal dissections. Y.J., K.L. and D.C. performed immunostaining. Y.J. and S.B. performed preliminary explant experiments. L.C.S. assisted with qPCR. Y.J., F.G.S., Z.M., L.Z. and H.B. wrote the manuscript.

## Competing Interests

The authors declare no competing interests.

## Reference

1 Takahashi, K. *et al.* Induction of pluripotent stem cells from adult human fibroblasts by defined factors. *Cell* **131**, 861-872, doi:10.1016/j.cell.2007.11.019 (2007).

2 Morizane, A. *et al.* Direct comparison of autologous and allogeneic transplantation of iPSC-derived neural cells in the brain of a non-human primate. *Stem Cell Reports* **1**, 283-292, doi:10.1016/j.stemcr.2013.08.007 (2013).

3 Iaccarino, C., Carretta, A., Nicolosi, F. & Morselli, C. Epidemiology of severe traumatic brain injury. *J Neurosurg Sci* **62**, 535-541, doi:10.23736/S0390-5616.18.04532-0 (2018).

4 Dewan, M. C. *et al.* Estimating the global incidence of traumatic brain injury. *J Neurosurg*, 1-18, doi:10.3171/2017.10.JNS17352 (2018).

5 Song, S. Y., Lee, S. K., Eom, K. S. & Investigators, K. Analysis of Mortality and Epidemiology in 2617 Cases of Traumatic Brain Injury : Korean Neuro-Trauma Data Bank System 2010-2014. *J Korean Neurosurg Soc* **59**, 485-491, doi:10.3340/jkns.2016.59.5.485 (2016).

6 Hall, K. M. Establishing a national traumatic brain injury information system based upon a unified data set. *Archives of physical medicine and rehabilitation* **78**, S5-S11 (1997).

7 Galgano, M. *et al.* Traumatic Brain Injury: Current Treatment Strategies and Future Endeavors. *Cell Transplant* **26**, 1118-1130, doi:10.1177/0963689717714102 (2017).

8 Espuny-Camacho, I. *et al.* Human Pluripotent Stem-Cell-Derived Cortical Neurons Integrate Functionally into

bioRxiv preprint doi: https://doi.org/10.1101/2022.10.28.513987; this version posted October 30, 2022. The copyright holder for this preprint (which was not certified by peer review) is the author/funder. All rights reserved. No reuse allowed without permission.

the Lesioned Adult Murine Visual Cortex in an Area-Specific Way. *Cell Rep* **23**, 2732-2743, doi:10.1016/j.celrep.2018.04.094 (2018).

9 Mansour, A. A. *et al.* An in vivo model of functional and vascularized human brain organoids. *Nat Biotechnol* **36**, 432-441, doi:10.1038/nbt.4127 (2018).

10 Harris, J. A. *et al.* Hierarchical organization of cortical and thalamic connectivity. *Nature* **575**, 195-202, doi:10.1038/s41586-019-1716-z (2019).

11 Barrett, L. F. & Simmons, W. K. Interoceptive predictions in the brain. *Nat Rev Neurosci* **16**, 419-429, doi:10.1038/nrn3950 (2015).

12 Harris, K. D. & Shepherd, G. M. The neocortical circuit: themes and variations. *Nat Neurosci* **18**, 170-181, doi:10.1038/nn.3917 (2015).

13 Kowalczyk, T. *et al.* Intermediate Neuronal Progenitors (Basal Progenitors) Produce Pyramidal–Projection Neurons for All Layers of Cerebral Cortex. *Cerebral Cortex* **19**, 2439-2450, doi:10.1093/cercor/bhn260 (2009).

14 Villar, G., Graham, A. D. & Bayley, H. A tissue-like printed material. *Science* **340**, 48-52, doi:10.1126/science.1229495 (2013).

15 Zhou, L. *et al.* Lipid-Bilayer-Supported 3D Printing of Human Cerebral Cortex Cells Reveals Developmental Interactions. *Adv Mater* **32**, e2002183, doi:10.1002/adma.202002183 (2020).

16 Alcinesio, A. *et al.* Controlled packing and single-droplet resolution of 3D-printed functional synthetic tissues. *Nat Commun* **11**, 2105, doi:10.1038/s41467-020-15953-y (2020).

17 Mota, B. & Herculano-Houzel, S. BRAIN STRUCTURE. Cortical folding scales universally with surface area and thickness, not number of neurons. *Science* **349**, 74-77, doi:10.1126/science.aaa9101 (2015).

18 Shen, Q. *et al.* The timing of cortical neurogenesis is encoded within lineages of individual progenitor cells. *Nature Neuroscience* **9**, 743-751, doi:10.1038/nn1694 (2006).

19 Gaspard, N. *et al.* An intrinsic mechanism of corticogenesis from embryonic stem cells. *Nature* **455**, 351-357, doi:10.1038/nature07287 (2008).

20 Shi, Y., Kirwan, P., Smith, J., Robinson, H. P. C. & Livesey, F. J. Human cerebral cortex development from pluripotent stem cells to functional excitatory synapses. *Nature Neuroscience* **15**, 477-486, doi:10.1038/nn.3041 (2012).

21 Haenseler, W. *et al.* A Highly Efficient Human Pluripotent Stem Cell Microglia Model Displays a Neuronal-Co-culture-Specific Expression Profile and Inflammatory Response. *Stem Cell Reports* **8**, 1727-1742, doi:10.1016/j.stemcr.2017.05.017 (2017).

22 Dovey, H. F. *et al.* Functional gamma-secretase inhibitors reduce beta-amyloid peptide levels in brain. *J Neurochem* **76**, 173-181, doi:10.1046/j.1471-4159.2001.00012.x (2001).

23 Sastre, M. *et al.* Presenilin-dependent γ-secretase processing of β-amyloid precursor protein at a site corresponding to the S3 cleavage of Notch. *EMBO reports* **2**, 835-841 (2001).

24 Louvi, A. & Artavanis-Tsakonas, S. Notch signalling in vertebrate neural development. *Nature Reviews Neuroscience* **7**, 93-102 (2006).

25 Crawford, T. Q. & Roelink, H. The notch response inhibitor DAPT enhances neuronal differentiation in embryonic stem cell-derived embryoid bodies independently of sonic hedgehog signaling. *Developmental dynamics: an official publication of the American Association of Anatomists* **236**, 886-892 (2007).

26 Qi, Y. *et al.* Combined small-molecule inhibition accelerates the derivation of functional cortical neurons from human pluripotent stem cells. *Nat Biotechnol* **35**, 154-163, doi:10.1038/nbt.3777 (2017).

27 Boissart, C. *et al.* Differentiation from human pluripotent stem cells of cortical neurons of the superficial layers amenable to psychiatric disease modeling and high-throughput drug screening. *Translational Psychiatry* **3**, e294-e294, doi:10.1038/tp.2013.71 (2013).

28 Rakic, P. Neurons in Rhesus Monkey Visual Cortex: Systematic Relation between Time of Origin and Eventual Disposition. *Science* **183**, 425-427, doi:10.1126/science.183.4123.425 (1974).

29 Taupin, P. *et al.* FGF-2-responsive neural stem cell proliferation requires CCg, a novel autocrine/paracrine cofactor. *Neuron* **28**, 385-397, doi:10.1016/s0896-6273(00)00119-7 (2000).

30 Lim, J. Y. *et al.* Brain-derived neurotrophic factor stimulates the neural differentiation of human umbilical cord blood-derived mesenchymal stem cells and survival of differentiated cells through MAPK/ERK and PI3K/Akt-dependent signaling pathways. *J Neurosci Res* **86**, 2168-2178, doi:10.1002/jnr.21669 (2008).

31 Zhang, X. *et al.* Pax6 is a human neuroectoderm cell fate determinant. *Cell stem cell* **7**, 90-100 (2010).

bioRxiv preprint doi: https://doi.org/10.1101/2022.10.28.513987; this version posted October 30, 2022. The copyright holder for this preprint (which was not certified by peer review) is the author/funder. All rights reserved. No reuse allowed without permission.


32 Park, D. *et al.* Nestin is required for the proper self-renewal of neural stem cells. *Stem cells* **28**, 2162-2171 (2010).

33 Mason, J. O. & Price, D. J. Building brains in a dish: Prospects for growing cerebral organoids from stem cells. *Neuroscience* **334**, 105-118, doi:https://doi.org/10.1016/j.neuroscience.2016.07.048 (2016).

34 Renner, M. *et al.* Self-organized developmental patterning and differentiation in cerebral organoids. *The EMBO Journal* **36**, 1316-1329, doi:https://doi.org/10.15252/embj.201694700 (2017).

35 Wolf, M. K. Anatomy of cultured mouse cerebellum. II. Organotypic migration of granule cells demonstrated by silver impregnation of normal and mutant cultures. *Journal of Comparative Neurology* **140**, 281-297 (1970).

36 Humpel, C. Organotypic brain slice cultures: A review. *Neuroscience* **305**, 86-98, doi:https://doi.org/10.1016/j.neuroscience.2015.07.086 (2015).

37 Bardy, C. *et al.* Neuronal medium that supports basic synaptic functions and activity of human neurons in vitro. *Proceedings of the National Academy of Sciences* **112**, E2725-E2734, doi:doi:10.1073/pnas.1504393112 (2015).

38 Chen, X. *et al.* High Glucose Inhibits Neural Stem Cell Differentiation Through Oxidative Stress and Endoplasmic Reticulum Stress. *Stem Cells Dev* **27**, 745-755, doi:10.1089/scd.2017.0203 (2018).

39 Yu, T. W. & Bargmann, C. I. Dynamic regulation of axon guidance. *Nat Neurosci* **4 Suppl**, 1169-1176, doi:10.1038/nn748 (2001).

40 Myers, J. P., Santiago-Medina, M. & Gomez, T. M. Regulation of axonal outgrowth and pathfinding by integrin-ECM interactions. *Dev Neurobiol* **71**, 901-923, doi:10.1002/dneu.20931 (2011).

41 Science, A. I. f. B. Allen Mouse Brain Atlas. *Available from https://developingmouse.brain-map.org/experiment/thumbnails/100098039?image_type=nissl* (2004).

42 Heck, D. H., Thach, W. T. & Keating, J. G. On-beam synchrony in the cerebellum as the mechanism for the timing and coordination of movement. *Proceedings of the National Academy of Sciences* **104**, 7658-7663, doi:doi:10.1073/pnas.0609966104 (2007).

43 Grienberger, C. & Konnerth, A. Imaging calcium in neurons. *Neuron* **73**, 862-885, doi:10.1016/j.neuron.2012.02.011 (2012).

44 Dupont, E., Hanganu, I. L., Kilb, W., Hirsch, S. & Luhmann, H. J. Rapid developmental switch in the mechanisms driving early cortical columnar networks. *Nature* **439**, 79-83, doi:10.1038/nature04264 (2006).

45 Ko, H. *et al.* Functional specificity of local synaptic connections in neocortical networks. *Nature* **473**, 87-91, doi:10.1038/nature09880 (2011).

46 Karra, D. & Dahm, R. Transfection Techniques for Neuronal Cells. *The Journal of Neuroscience* **30**, 6171, doi:10.1523/JNEUROSCI.0183-10.2010 (2010).

47 Skylar-Scott, M. A. *et al.* Orthogonally induced differentiation of stem cells for the programmatic patterning of vascularized organoids and bioprinted tissues. *Nat Biomed Eng*, doi:10.1038/s41551-022-00856-8 (2022).

48 Milone, M. C. & O'Doherty, U. Clinical use of lentiviral vectors. *Leukemia* **32**, 1529-1541, doi:10.1038/s41375-018-0106-0 (2018).

49 Matsushita, M. *et al.* Neural differentiation of human embryonic stem cells induced by the transgene-mediated overexpression of single transcription factors. *Biochemical and Biophysical Research Communications* **490**, 296-301, doi:https://doi.org/10.1016/j.bbrc.2017.06.039 (2017).

50 Linaro, D. *et al.* Xenotransplanted Human Cortical Neurons Reveal Species-Specific Development and Functional Integration into Mouse Visual Circuits. *Neuron* **104**, 972-986.e976, doi:10.1016/j.neuron.2019.10.002 (2019).

51 Agnati, L. F. *et al.* A correlation analysis of the regional distribution of central enkephalin and β-endorphin immunoreactive terminals and of opiate receptors in adult and old male rats. Evidence for the existence of two main types of communication in the central nervous system: the volume transmission and the wiring transmission. *Acta Physiologica Scandinavica* **128**, 201-207 (1986).

52 Agnati, L. F., Guidolin, D., Guescini, M., Genedani, S. & Fuxe, K. Understanding wiring and volume transmission. *Brain Research Reviews* **64**, 137-159, doi:https://doi.org/10.1016/j.brainresrev.2010.03.003 (2010).

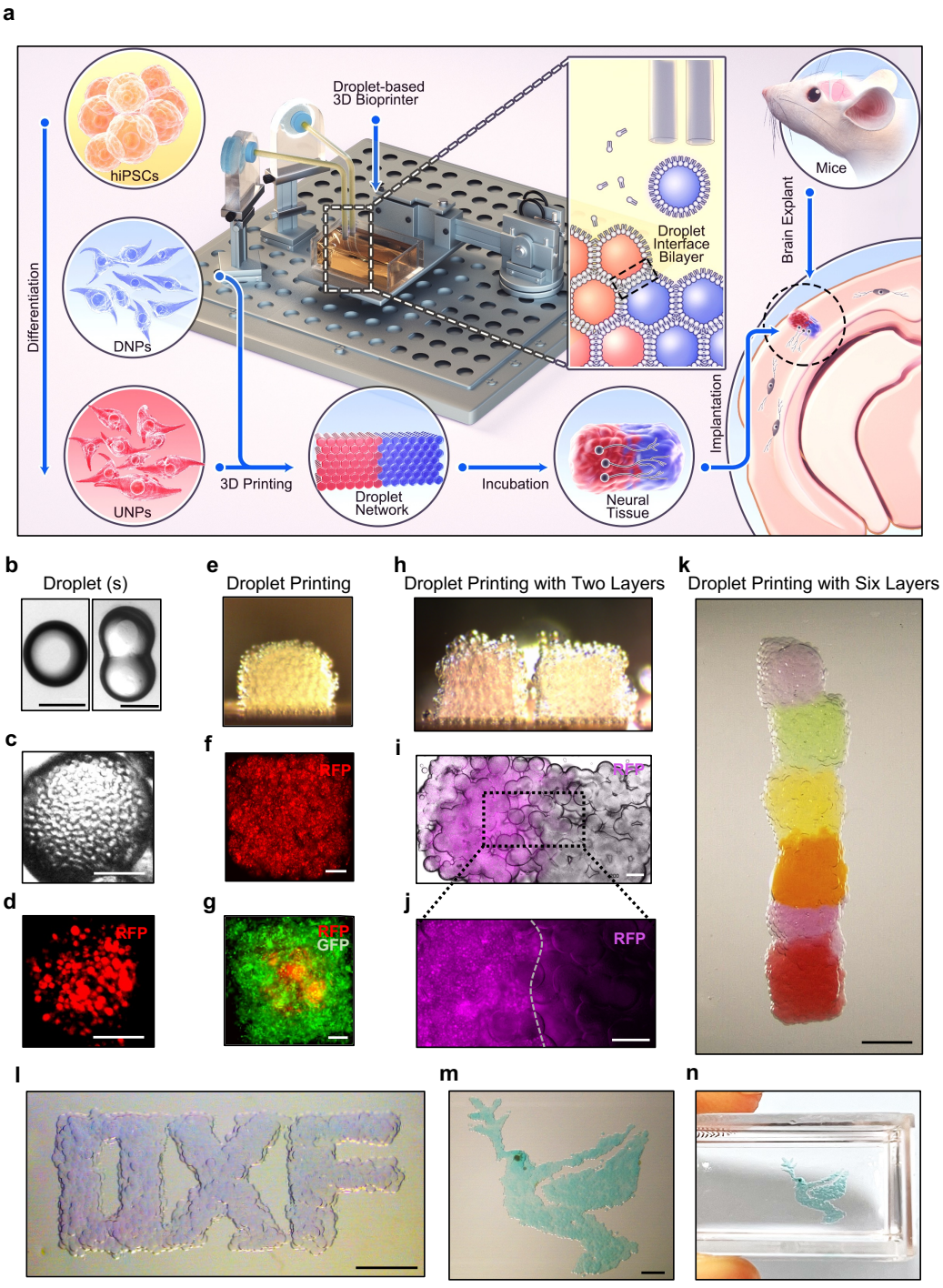
a
hiPSCs
DNPs
UNPs
Differentiation
Droplet-based
3D Bioprinter
3D Printing
Droplet
Network
Incubation
Neural
Tissue
Droplet
Interface
Bilayer
Mice
Brain Explant
Implantation
b
Droplet (s)
e
Droplet Printing
h
Droplet Printing with Two Layers
k
Droplet Printing with Six Layers
c
f
RFP
i
RFP
d
RFP
g
RFP
GFP
j
RFP
l
m
n

**Fig. 1: Droplet-based 3D bioprinting. a.** Overview of the study. Patterned 3D printing of droplets containing the hiPSC-derived neural progenitors, deep-layer neural progenitors (DNPs) and upper-layer neural progenitors (UNPs), and extracellular matrix (ECM). The formation of adhesive DIBs secured the patterned network. The printed cerebral cortical tissues were cultured *in vitro* for functional studies and implanted into mouse brain explants. **b.** Bright-field images of a single droplet (left) and a pair of droplets connected through a DIB (right). The droplets consist of solidified ECM. **c.** and **d.** Image of a droplet printed with RFP-labelled DNPs in ECM. **e.** Side-view of an 8x8x8 printed droplet network containing DNPs. **f.** Image of a printed droplet network containing RFP-labelled DNPs. **g.** Image of a patterned droplet network containing GFP-labelled 3T3 cells (outer compartment) and RFP-labelled MDA breast cancer cells (centre compartment). **h.** Side-view of a printed 16x8x8 droplet network containing two layers (left and right). **i.** Image of a printed two-layer droplet network containing RFP-labelled UNPs (left) and unlabelled DNPs (right). **j.** Fluorescence image of a section of **'i'** (indicated by the dashed box) at higher magnification. **k.** Image of a printed 6-layered droplet network resembling the structure of a cortical column. **l, m** and **n.** Images of centimetre-sized droplet networks. Scale bars: **'b'** & **'d'**, 100 μm; **'f'**, **'g'**, **'i'** & **'j'**, 200 μm; **'k'**, **'l'**, **'m'** & **'n'**, 1000 μm.

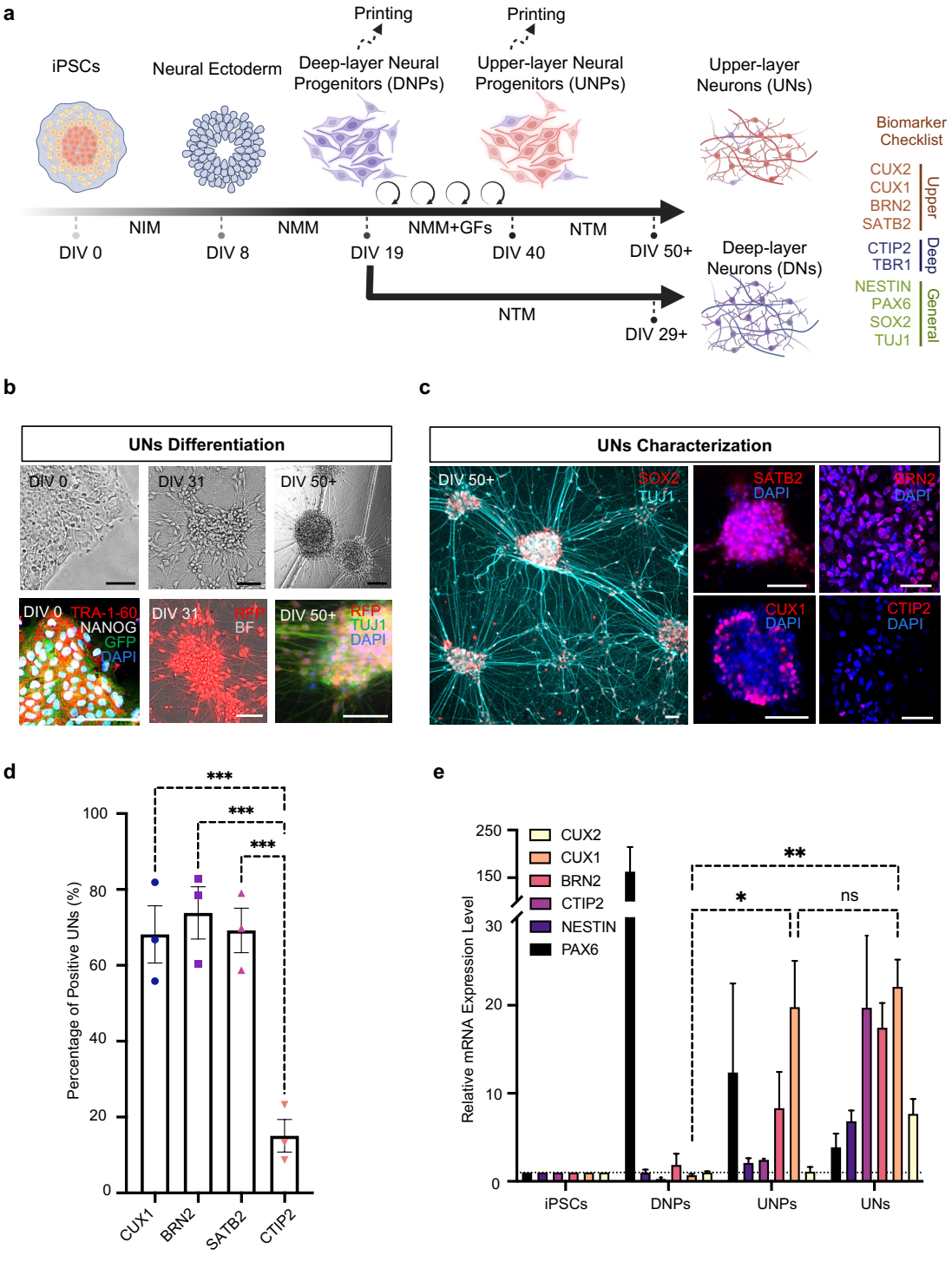
a
Printing
Printing
iPSCs
Neural Ectoderm
Deep-layer Neural Progenitors (DNPs)
Upper-layer Neural Progenitors (UNPs)
Upper-layer Neurons (UNs)
Biomarker Checklist
CUX2
CUX1
BRN2
SATB2
Upper
CTIP2
TBR1
Deep
NESTIN
PAX6
SOX2
TUJ1
General
NIM
NMM
NMM+GFs
NTM
DIV 0
DIV 8
DIV 19
DIV 40
DIV 50+
Deep-layer Neurons (DNs)
NTM
DIV 29+
b
UNs Differentiation
DIV 0
DIV 31
DIV 50+
DIV 0 TRA-1-60 NANOG GFP DAPI
DIV 31 RFP BF
DIV 50+ RFP TUJ1 DAPI
c
UNs Characterization
DIV 50+ SOX2 TUJ1
SATB2 DAPI
BRN2 DAPI
CUX1 DAPI
CTIP2 DAPI
d
Percentage of Positive UNs (%)
100
80
60
40
20
0
***
***
***
CUX1
BRN2
SATB2
CTIP2
e
Relative mRNA Expression Level
250
150
30
20
10
0
CUX2
CUX1
BRN2
CTIP2
NESTIN
PAX6
**
*
ns
iPSCs
DNPs
UNPs
UNs

842

**Fig. 2: Generation of layer-specific neural cells. a.** Schematic showing the differentiation timeline of hiPSCs to DNs and UNs, via the corresponding progenitors: DNPs and UNPs. Abbreviations: Day in vitro (DIV); Neural Induction Medium (NIM); Neural Maintenance Medium (NMM), Neural Terminal Medium (NTM); Growth Factors (GFs). DIV 0-8: hiPSCs induction, committing to a neural ectoderm lineage; DIV 8-19: neural ectoderm cells differentiating into DNPs; DIV 19-40: DNPs differentiating to UNPs during extended culture in NMM supplemented with growth factors (FGF-2, EGF and BDNF). DIV 19-29+ and DIV 40-50+, DNPs and UNPs maturing as DNs and UNs, respectively. **b.** Bright-field images (top row) and immunocytochemistry images (bottom row) of cells at different stages of differentiation: DIV 0, 31, 50+, correspond to hiPSCs, NPs and UNs respectively. **c.** Immunocytochemistry analysis of the young neuron marker β3-tubulin (labelled with the TUJ1 antibody), the neural stem cell marker (SOX2), middle-upper layer marker (SATB2), upper layer markers (CUX1 and BRN2) and the deep layer marker (CTIP2) expression in differentiated UNs. See Extended Data Fig.3b for further immunocytochemistry analysis of DNs. **d.** Quantification of marker expression in c. (n = 3; one-way ANOVA test.) **e.** Quantitative RT-PCR analysis of upper layer markers (CUX1, CUX2 & BRN2), deep layer marker (CTIP2), neurofilament marker (NESTIN) and neuroectoderm marker (PAX6). Marker expression of indicated cell types related to hiPSCs. (n = 3; one-way ANOVA test). For **'b'** and **'c'**, scale bar, 50 μm. For both **'d'** and **'e'**, ns = not significant. *, $P < 0.05$, **, $P < 0.01$ and ***, $P < 0.001$.

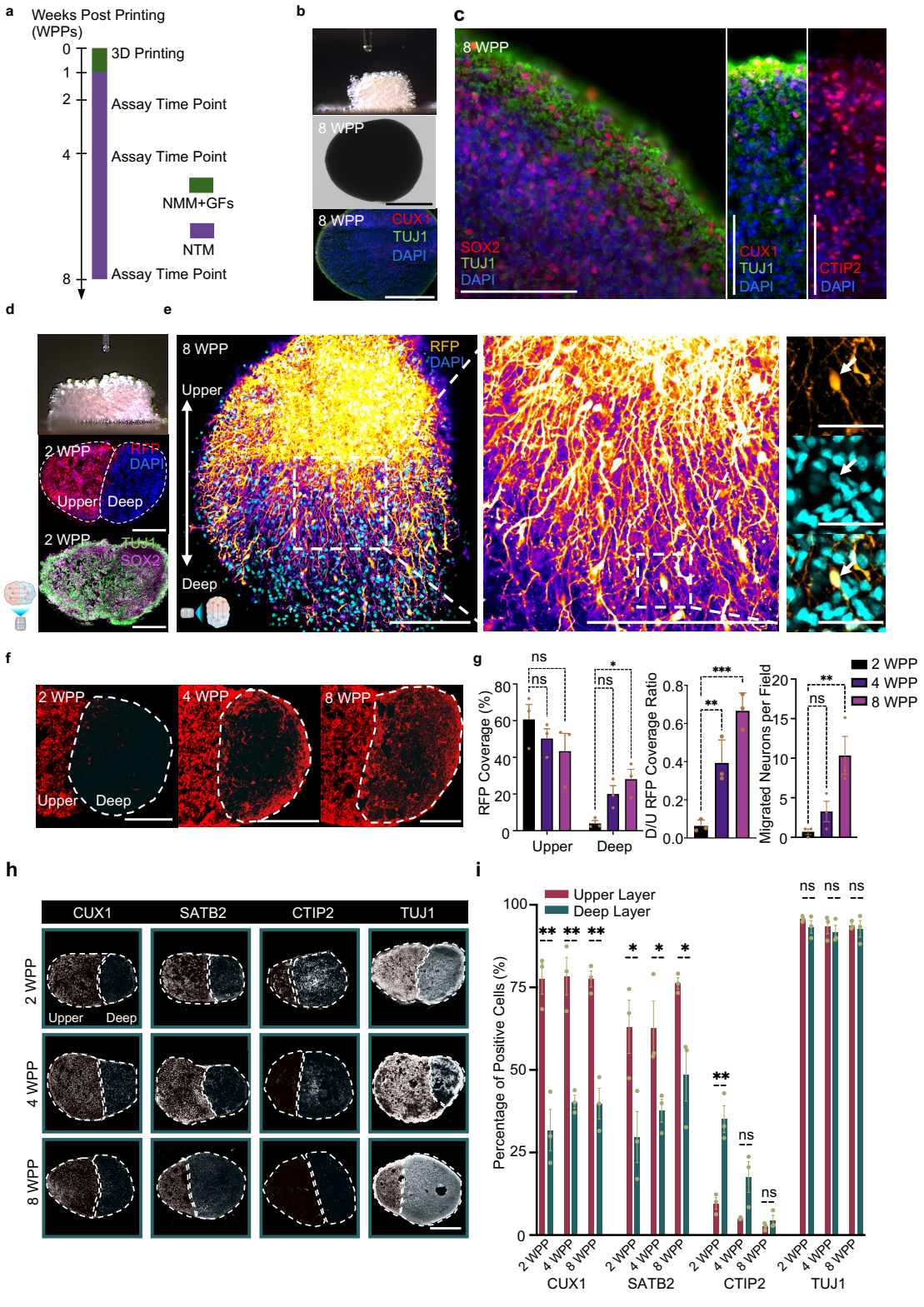
a
Weeks Post Printing (WPPs)
0
1
2
4
8
3D Printing
Assay Time Point
Assay Time Point
NMM+GFs
NTM
Assay Time Point
b
8 WPP
8 WPP
CUX1
TUJ1
DAPI
c
8 WPP
SOX2
TUJ1
DAPI
CUX1
TUJ1
DAPI
CTIP2
DAPI
d
2 WPP
RFP
DAPI
Upper
Deep
2 WPP
TUJ1
SOX2
e
8 WPP
RFP
DAPI
Upper
Deep
f
2 WPP
4 WPP
8 WPP
Upper
Deep
g
RFP Coverage (%)
D/U RFP Coverage Ratio
Migrated Neurons per Field
Upper
Deep
2 WPP
4 WPP
8 WPP
ns
*
**
***
h
CUX1
SATB2
CTIP2
TUJ1
2 WPP
4 WPP
8 WPP
Upper
Deep
i
Upper Layer
Deep Layer
Percentage of Positive Cells (%)
CUX1
SATB2
CTIP2
TUJ1
2 WPP
4 WPP
8 WPP
ns
*
**

863

**Fig. 3: Construction of cerebral cortical tissue with deep and upper layers. a.** Timeline for the production and *in vitro* culture of droplet-printed cortical tissues. Further details are described in Methods. **b.** Side view of an ongoing printing process (top), bright-field image of the deep layer cortical tissue after 8 weeks post-printing (WPP) (middle), and fluorescence immunostaining of sectioned 8 WPP tissue (bottom). **c.** Fluorescence images of sectioned 8 WPP deep-layer cortical tissue showing the expression of stem (SOX2), young neuronal (TUJ1) and layer-specific markers (CUX1, CTIP2 & TBR1). Scale bars, 100 μm. **d.** Printing of two-layer cortical tissues. Side view of a printed two-layer cortical tissue (top), and fluorescence images of a sectioned 2 WPP two-layer tissue (middle and bottom). **e.** Confocal z-projection image (left) and the magnified image (middle and right) showing cross-layer process outgrowth and neuron migration in a printed two-layer tissue at 8 WPP, visualized by RFP (false coloured as fire) expression in UNs and DAPI nucleus staining in both UN and DNs. Arrow indicates a migrating UN. Scale bars: left and middle, 500 μm; right, 50 μm. **f.** Fluorescence images of cortical tissue sections with cross-layer process outgrowth and cell migration at 2 (left), 4 (middle) and 8 (right) WPP. Dashed circles indicating the deep-layer segment with invading RFP-labelled UNs. Scale bars, 200 μm. **g.** Quantitative analysis of process outgrowth by RFP coverage (left and middle), and neuron migration by cell body counting (right), as showed in 'f' (n = 3, one-way ANOVA test). Field size, 0.1mm$^2$. **h.** Spatiotemporal immunofluorescence analysis of general neural and layer-specific marker expression on sectioned two-layer cortical tissues. Dashed line outlines the layers. **i.** Quantitative analysis of marker expression in upper and deep layers of cortical tissues in '**h**' (n = 3; unpaired student t test). ns = not significant; *, P < 0.05; **, P < 0.01; ***, P < 0.001. Sections thickness: 30 μm. For '**b**', '**d**' & '**h**': scale bars, 500 μm.

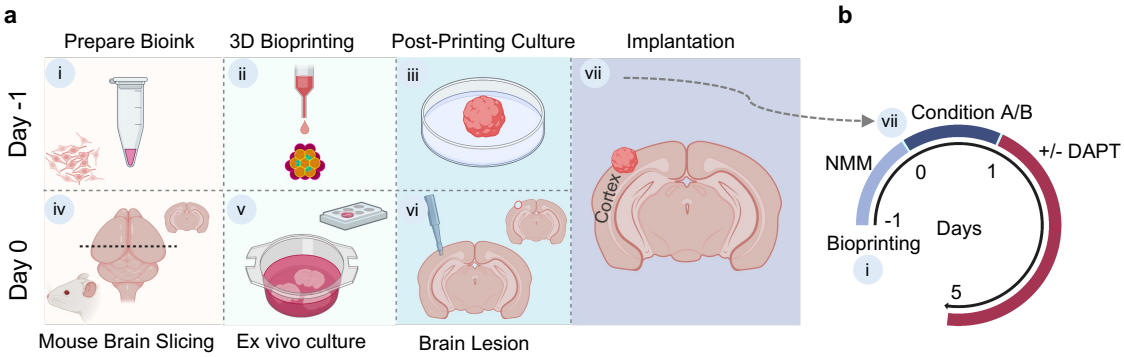
a
Prepare Bioink
3D Bioprinting
Post-Printing Culture
Implantation
Day -1
Day 0
Mouse Brain Slicing
Ex vivo culture
Brain Lesion
b
Condition A/B
+/- DAPT
NMM
Bioprinting
Days
Cortex

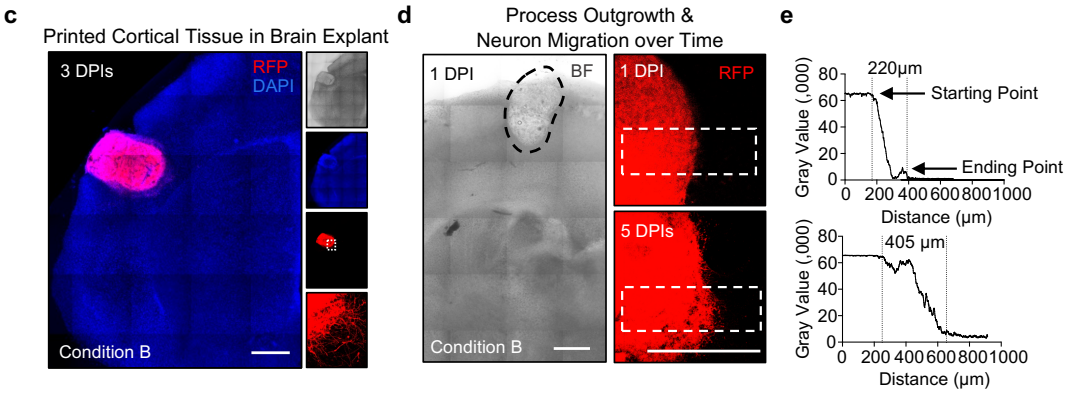
c
Printed Cortical Tissue in Brain Explant
3 DPIs
RFP
DAPI
Condition B
d
Process Outgrowth &
Neuron Migration over Time
1 DPI
BF
RFP
5 DPIs
e
220µm
Starting Point
Ending Point
Gray Value (,000)
Distance (µm)
405 µm

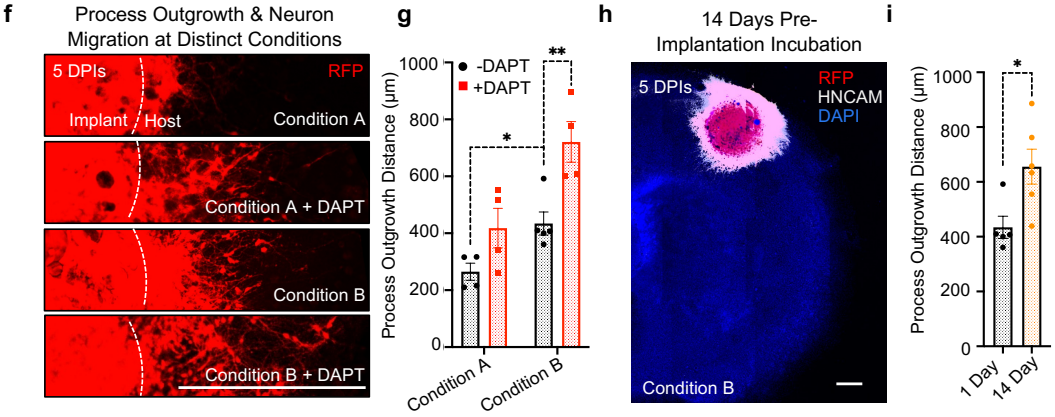
f
Process Outgrowth & Neuron
Migration at Distinct Conditions
5 DPIs
RFP
Implant
Host
Condition A
Condition A + DAPT
Condition B
Condition B + DAPT
g
-DAPT
+DAPT
Process Outgrowth Distance (µm)
Condition A
Condition B
h
14 Days Pre-
Implantation Incubation
HNCAM
DAPI
i
1 Day
14 Day

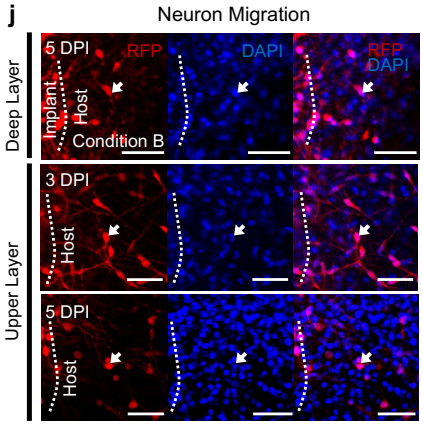
j
Neuron Migration
Deep Layer
Upper Layer
5 DPI
3 DPI
RFP
DAPI
Implant
Host
Condition B

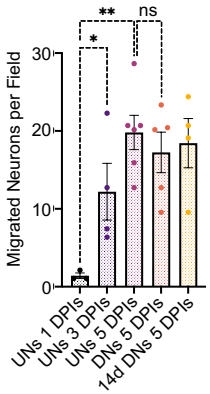
k
Migrated Neurons per Field
ns
UNs 1 DPIs
UNs 3 DPIs
UNs 5 DPIs
DNs 5 DPIs
14d DNs 5 DPIs

888

**Fig. 4: Implantation of printed single-layer cortical tissue into brain explants. a.** Steps in the implantation process. Step i, bioink prepared from DNPs or/and UNPs with Matrigel. Step ii, droplet-printing of cortical tissue. Step iii, post-printing culture of the printed tissue for 1 day. Step iv, preparation of mouse brain slices with a thickness of 300 µm. Step v, brain slices (explants) were kept under condition A or condition B before implantation. Step vi, creating the brain lesion with a biopsy punch. Step vii, implanting printed tissue into the lesion of the explant, which was then further incubated. **b.** Incubation of the implanted explant and drug treatment. Explants were incubated under either condition A or condition B for 1 day, followed by treatment with or without DAPT for 4 days. **c.** Left, tiled fluorescence confocal image of an implanted mouse brain explant at 3 days post implantation (DPIs) under condition B. The implant contained RFP-labelled DNs. Right, bright field (top), DAPI staining (upper middle), RFP-labelled implanted tissue (lower middle) and higher magnification view (bottom). The culture media are described in Methods. **d.** Confocal image of a representative 1 DPI implanted explant (left) and confocal fluorescence live images of process outgrowth and neuron migration from an explant at 1 (top right) and 5 (bottom right) DPI. **e.** Profile plots of fluorescence intensity along the white dashed boxes from left to right indicated in **'d'**. The vertical dashed lines indicate the margins of the red fluorescence. **f.** Confocal images of implant-to-host process outgrowth and neuron migration at 5 DPIs. The implanted explants were cultured under the two conditions and with or without DAPT treatment. Dashed lines indicate the original borders of the implants. **g.** Quantitative analysis of process outgrowth and neuron migration distance showed in **'f'**. ($n \geqslant 4$; unpaired student t tests). **h.** A tiled confocal image of an explant implanted with deep-layer cortical tissue that had been cultured for 14 days prior to implantation. The implant is immunostained with the human-specific neural marker, HNCAM. RFP localisation indicates process outgrowth and neuron migration from the implanted tissue. **i.** Quantitative analysis of process outgrowth and neuron migration from deep-layer cortical tissue cultured for 1 day or 14 days prior to implantation ($n \geqslant 4$; unpaired student t test). **j.** Representative confocal images of an explant with DNs at 5 DPI (top), and explants with UNs at 3 DPI (middle) and 5 DPI (bottom), revealing the migration of RFP-labelled neurons from implanted cortical tissues into the brain explants. Arrow indicates a migrating human neuron. Scale bar, 50 µm. **k.** Quantitative analysis of

neuron migration from implanted cortical tissues into host brain explants (n ⩾3; one-way ANOVA). Field size, 0.1mm$^2$. For '**g**', '**i**' & '**k**': ns = not significant; *, P < 0.05; **, P < 0.01. For **'c', 'd', 'f' & 'h'**: scale bars, 500 μm.

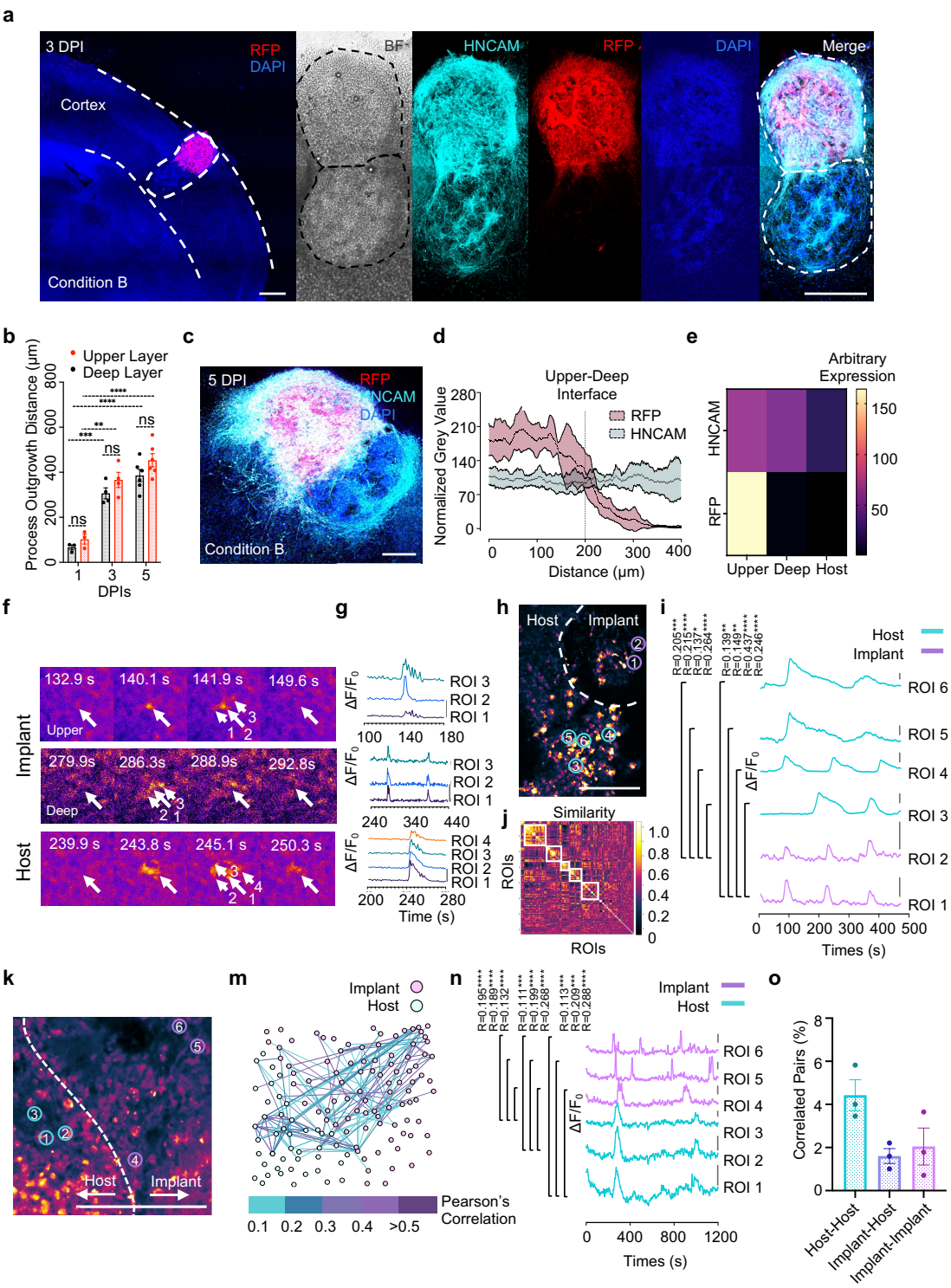
a
3 DPI
RFP
DAPI
Cortex
Condition B
BF
HNCAM
RFP
DAPI
Merge
b
Upper Layer
Deep Layer
Process Outgrowth Distance (μm)
DPIs
c
5 DPI
RFP
HNCAM
DAPI
Condition B
d
Upper-Deep Interface
RFP
HNCAM
Normalized Grey Value
Distance (μm)
e
Arbitrary Expression
HNCAM
RFP
Upper Deep Host
f
Implant
Host
Upper
Deep
g
ROI 3
ROI 2
ROI 1
ROI 4
Time (s)
h
Host
Implant
i
Host
Implant
ROI 6
ROI 5
ROI 4
ROI 3
ROI 2
ROI 1
Times (s)
j
Similarity
ROIs
k
Host
Implant
m
Implant
Host
Pearson's Correlation
n
Implant
Host
Times (s)
o
Correlated Pairs (%)
Host-Host
Implant-Host
Implant-Implant

923

**Fig. 5. Functional activity of two-layer cortical tissue and integration with the host explant. a.** Tiled fluorescence confocal image of implanted explant at 3 DPI. Dashed lines delineate cerebral cortex of the mouse and the implanted tissue. The human specific neural marker HNCAM labels both layers of the implanted tissue while RFP only labels the upper layer. **b.** Quantitative analysis of process outgrowth and neuron migration from the two-layered tissues into the brain explant on 1, 3 and 5 DPIs ($n \geqslant 3$; ns = not significant; ***, $P < 0.001$; ****, $P < 0.0001$; unpaired student t tests). **c.** A tiled fluorescence confocal image of a two-layer implant at 5 DPIs. **d.** Fluorescence-intensity profiles showing HNCAM expression in both layers of the printed tissue, while RFP expression falls off in the deep layer ($n \geqslant 3$) **e.** Heatmap showing marker expression by grey value in the upper and deep layers of a tissue implant and in the host at 5 DPI ($n \geqslant 3$). **f.** Video frames of Fluo-4 live calcium imaging of the implanted explants reveals spontaneous calcium oscillations (coloured as fire) in individual adjacent cells at 5 DPI. **g.** Single-cell Fluo-4 calcium traces. Regions of interest (ROIs) indicated by arrows in 'f'. **h.** Fluo-4 calcium imaging of an explant implanted with DNPs only at 5 DPI. Dashed line shows the interface of the implant and the host (see Supplementary Fig. 7a). **i.** Correlated single-cell calcium traces between implant and the host explant, colour-coded according to their ROIs as indicated in **'h'**. Scale bar: $\Delta F/F_0 = 0.8$. **j.** Similarity matrix showing communities of neurons with correlated firing patterns. Dashed boxes show neurons that tend to activate together. Colour indicates normalized correlation. **k.** Fluo-4 images of an explant implanted with UNPs only at 5 DPI. The dashed line shows the interface between the implant and the host (see Supplementary Fig. 7d). **m.** Correlated neuron pairs within **'k'**, between the implant and the host at 5 DPI by network analysis. Points representing neurons and the lines between them indicate correlated calcium signals. **n.** Single-cell calcium traces, colour-coded ROIs as indicated in **'k'**. Scale bar: $\Delta F/F_0 = 0.05$. **o.** Quantitative analysis of the correlated cell pairs within the host, within the implant and between the host and the implant. Signal pairs with Pearson's correlations over 0.1 are counted (n = 3). Slice thickness: 300 µm. For **'a'**, **'c'**, **'h'** and **'k'**: scale bars, 200 µm. For **'i'** & **'n'**. Pearson's correlation: *, $P<0.05$, **, $P<0.01$ ***, $P < 0.001$ and ****, $P < 0.0001$.